HHS Public Access

Author manuscript

Lab Chip. Author manuscript; available in PMC 2020 March 14.

Published in final edited form as:

Lab Chip. 2018 February 27; 18(5): 793–802. doi:10.1039/c7lc01300k.

Rapid flow in multilayer microfluidic paper-based analytical devices†

Robert B. Channon[‡,a], **Michael P. Nguyen**[‡,a], **Alexis G. Scorzelli**[b], **Elijah M. Henry**[a], **John Volckens**[c], **David S. Dandy**[d], **Charles S. Henry**[a]

[a]Department of Chemistry, Colorado State University, Fort Collins, Colorado 80523, USA.

[b]Department of Chemistry and Physics, Monmouth University, West Long Branch, New Jersey 07764, USA

[c]Department of Mechanical Engineering, Colorado State University, Fort Collins, Colorado 80523, USA

[d]Department of Chemical and Biological Engineering, Colorado State University, Fort Collins, Colorado 80523, USA

Abstract

Microfluidic paper-based analytical devices (μPADs) are a versatile and inexpensive point-of-care (POC) technology, but their widespread adoption has been limited by slow flow rates and the inability to carry out complex in field analytical measurements. In the present work, we investigate multilayer μPADs as a means to generate enhanced flow rates within self-pumping paper devices. Through optical and electrochemical measurements, the fluid dynamics are investigated and compared to established flow theories within μPADs. We demonstrate a ~145-fold increase in flow rate (velocity = 1.56 cm s^{-1}, volumetric flow rate = 1.65 mL min^{-1}, over 5.5 cm) through precise control of the channel height in a 2 layer paper device, as compared to archetypical 1 layer μPAD designs. These design considerations are then applied to a self-pumping sequential injection device format, known as a three-dimensional paper network (3DPN). These 3DPN devices are characterized through flow injection analysis of a ferrocene complex and anodic stripping detection of cadmium, exhibiting a 5× enhancement in signal compared to stationary measurements.

Introduction

The resurgence of point-of-care (POC) devices has transformed analytical science by enabling *in situ* detection of a wide range of analytes across a variety of measurement

†Electronic supplementary information (ESI) available: Fig. S1–S7 investigate the swelling in 2 and 3 layer μPADs, the velocity in multilayer μPADs with and without double sided sticky tape between the layers, with different orientations, with different paper types and with different volumes. Channel heights are estimated based on these velocities, and snapshot photographs of a multilayered 3DPN during sequential injection of $FcTMA^+$ are provided. See DOI: 10.1039/c7lc01300k

chuck.henry@colostate.edu.

‡RBC and MPN contributed equally to this work.

Conflicts of interest

There are no conflicts to declare.

domains.[1] POC devices are often characterized by their simple miniaturization and low-cost compared to traditional measurement technologies.[1] These features have brought quantification and treatment from centralized laboratories to home and field, resulting in significant enhancements in patient care.[1,2] However, high sensitivity, high selectivity and complex reaction schemes are challenging to implement in a POC format without adding cumbersome and/or expensive external equipment.[1–3]

Microfluidic paper-based analytical devices (μPADs) are an attractive POC platform, given their portability, disposability, simple fabrication with inexpensive materials, ease of use, ability to store reagents, and compatibility with a wide range of analytes.[4–7] Sample transport is generated through capillary action, circumventing the need for external pumps and reducing device cost and complexity.[8,9] Despite these advantages, μPADs face several significant challenges, including the effect of testing conditions (*e.g.* humidity),[10] reduced sensitivity[9] and selectivity,[11] sample loss,[12] and additional challenges associated with adapting POC technologies from the lab to the field.[13] In particular, low transport velocities within μPADs often result in long assay times (40–60 min),[8,14–18] which diminishes their effectiveness as POC assays.

Sample flow in μPADs is frequently described by the Lucas–Washburn equation,

$$l(t) = \sqrt{\frac{\gamma r t \cos\theta}{2\mu}} \quad (1)$$

where l is the distance traversed down the channel (m) at time t (s), γ is the interfacial tension (N m^{-1}), r is the mean capillary radius (m), θ is the fluid contact angle on the paper, and μ is the fluid viscosity (N s m^{-1}). Many experimental factors, such as sample volume, gravity, fiber swelling, viscous drag and evaporation effects are not treated within eqn (1),[5] and more comprehensive analytical[10,19–21] or computational[22] modeling is challenging, often requiring *ad hoc* variables to fit theory to experimental data.[10]

Control of sample flow rate in μPADs is critical for optimizing most assays. The slow to moderate flow rates common in μPADs result in slower data acquisition times compared to classical microfluidic devices (tens of minutes *versus* seconds). This limitation can be attributed to the paper substrates' ability to transport sample *via* capillary action. In some applications, lower flow rates may be desired, such as for enzymatic reactions that proceed slowly,[9,23] or immunoassays, which require slow antibody–antigen binding steps before detection.[24] However, fast flow rates are needed for measurement of quasi-stable species and for enhancement of electrochemical signals through increased mass transport.[9,10,25] Recently, μPADs have been developed with increased sample velocities through use of either hollow channels,[18,22] carved channels,[15] or multiple layers of paper through stacking or folding.[9,10,22,26] Hollow channels, in particular, have been shown to give a ~7× increase in flow rate compared to single-layered devices.[18] Many of these approaches, however, require the use of syringe pumps or head pressure to increase flow rates. Flow rates in μPADs are also complicated by evaporation,[10,27] changes in substrate properties (*e.g.*, pore size and fiber width) between different paper types,[4,28] and swelling of the paper fibers.[22] Although evaporation effects are often managed through sealing of devices with tape or lamination,

[5,9,10] the effect of this sealing on flow rates within μPADs has not been formally investigated, to the best of our knowledge.

Methods for the sequential injection of multiple reagents are critical for μPAD advancement.[14,29] However, slow flow rates, the need to introduce reagents in a specific order,[30] the requirement for different reaction times for different assay steps,[6] and manual manipulation errors[31] have made μPADs challenging to design, and difficult to use with rapid assay protocols. Sequential-injection μPADs have been developed to address this need,[17,23,32,33] most notably one- and two-dimensional paper networks (1DPN, 2DPN).[19,30,34] Unfortunately, many of the approaches described to date are impractical for POC settings (*i.e.*, operator instigation[35–37] or specific temperature or electrical signals to open or close valves[38]) and most designs still suffer from long reaction times and undue sample mixing between successive injections.[19] In summary, whilst several reports have investigated the introduction of multiple reagents and functionalities within μPADs, the fast and controlled sequential addition of multiple reagents remains a challenge.[14,17,39]

In this work, we present the design of multilayered μPADs that exhibit considerably higher flow rates than previously described.[30,33,34] We first characterize fundamental aspects of sample flow in these devices. We also describe the ability to apply these devices for timed, sequential injections in a self-pumping format, henceforth referred to as a three-dimensional paper network (3DPN). Through careful device design, the flow rate and injection sequence can be tuned for specific applications. Electrochemical detection and optical imaging are used to characterize the flow phenomena, leading to an improved understanding of flow within 3DPNs. The device's analytical potential is demonstrated by comparing square-wave anodic stripping analysis of cadmium in a paper-based spot test, a μPAD, and a 3DPN.

Experimental

Materials and equipment

Whatman grade 1 chromatography paper, Whatman grade 1 qualitative paper, and Whatman grade 4 qualitative paper were purchased from GE Healthcare sciences (UK). Scotch Heavy Duty Shipping packing tape (3 M) and Scotch Permanent double sided tape (3 M) were purchased from Office Max. Great Value FD&C Red 40 dye was purchased from Wal-Mart Stores, Inc. (Bentonville, AR). Conductive Ag paint was purchased from SPI supplies (West Chester, PA, USA). Potassium nitrate (KNO_3), ferric chloride ($FeCl_3{\cdot}6H_2O$), sodium hydroxide (KOH), and 30% hydrogen peroxide (H_2O_2) were purchased from Fisher Scientific (Fairlawn, NJ, USA). Cadmium$_{(II)}$ nitrate, bismuth$_{(III)}$ oxide and sodium acetate trihydrate were purchased from Sigma Aldrich (St. Louis, MO). Glacial acetic acid was purchased from EMD Millipore (Billerica, MA). Au and Ag microwires (both 25 μm diameter, 99.99% pure) were purchased from California Fine Wire Company (Grover Beach, CA, USA) and ferrocenylmethyltrimethylammonium hexafluorophosphate ($FcTMA^+$) was synthesized according to a previously described procedure.[40] All solutions were prepared in ultrapure Milli-Q water (18.2 MΩ cm, MilliPore, MA, USA). The humidity in the laboratory varied between 25 and 40% from day to day. Nothing was done to control humidity during experiments. All devices were printed with a Xerox ColorQube 8870 wax printer (Norwalk, CT, USA), and lamination was performed with an Apache AL 13P thermal laminator. Paper

and tape segments were cut with a 30 W Epilog Zing Laser Cutter and Engraver (Golden, CO, USA) for device fabrication.

Device fabrication

Two multilayer μPAD designs were tested, namely straight channel and 3DPN devices, as illustrated in Fig. 1 and 7a respectively. All devices were designed in CorelDRAW X4 (Ottawa, Ontario, CAN), fabricated from Whatman 1 chromatography paper (thickness = 96 μm, mean capillary radius = 0.22 μm) and printed with "Sky Blue" ($R = 0$, $G = 124$, $B = 195$) colored wax (Fig. 1-ii). To confine the fluid flow, hydro-phobic wax barriers were created by melting wax printed devices on a hot plate (Fisher Scientific IsoTemp) at 150 °C for 90 s. The μPADs all featured a channel width of 4.52 mm after printing and melting the wax barriers. Each device was then laser cut using a CO_2 engraver (Epilog, Golden, CO) to individually separate them. Multilayer paper devices were held together with double sided tape (78 μm thickness, Fig. 1-iii); the distances between the multiple sheets of paper were varied by stacking multiple layers of double sided tape between them (78 μm increments). The double-sided tape was hand cut to fit the outside of the paper channel on the wax region of the device (Fig. 1-ii). Unless otherwise stated, packing tape was used to seal the outside of the μPADs and 3DPNs (Fig. 1-i), the μPADs were held vertically (90° relative to the benchtop), and experiments were started by lowering the device onto microwells containing the dye or electrochemical mediators.

Electrochemical and image analysis

All electrochemical measurements were carried out with a CH Instruments 1242B model potentiostat (Bee Cave, TX, USA) with an Au microwire working electrode. For $FcTMA^+$ oxidation, and Ag/AgCl reference/counter electrode was used in a 2 electrode setup.[9] For stripping analysis, three Au electrodes were used as working, pseudo-reference and counter electrodes in a 3 electrode setup. Before use, fresh Au microwires were cut and cleaned by submerging in a solution containing 25% H_2O_2 and 50 mM KOH for 20 min, followed by submerging in ultra-pure water for 5 min.[41] Ag/AgCl reference electrodes were fabricated by submerging an Ag microwire in 50 mM $FeCl_3$ for 50 s then submerging in ultrapure water for 5 min.[42] All videos and pictures were recorded with an Nikon Coolpix L110 camera and analyzed in MPC-HC (Windows). Conductive Ag paint was used to make an Ohmic contact between the microwire and the potentiostat's alligator clips. Square-wave anodic stripping voltammetry was carried out through deposition at −1.6 V *vs.* an Au reference electrode for different times based on the device format. Square wave stripping voltammetry was carried out after a 10 s equilibration time, scanning from −1.5 to 0 V, with a 15 mV a step potential, 75 mV amplitude and 10 Hz frequency.

Results and discussion

Investigation of sealing method

As highlighted by various research groups, the sealing method can have significant effects on flow in μPADs.[10,17,43] Therefore, the flow rate in straight channel μPADs was investigated using packing tape, lamination and an unsealed control (open) for 1 layer of paper μPADs. Flow rates were calculated by monitoring the time the fluid front from of a

150 μL aliquot of diluted food dye traversed a straight channel μPAD. As shown in Fig. 2a, significantly faster flow rates are observed for taped (0.014 cm s^{-1}) over both open (0.0057 cm s^{-1}) and laminated devices (0.0033 cm s^{-1}), for distances up to 4.2 cm (statistically significant based on an unpaired *t* test $p < 0.05$). Slower flow rates are expected in the open device, as evaporation leads to a significant reduction in flow rate over longer distances.[10] We attribute the faster flow rates in taped devices over laminated ones to the generation of micro-pores between the tape and paper, which are not present in lamination due to a tighter seal.[9] In fact, flow in the open and laminated devices had completely ceased by ~4.5 cm. Additionally, it has been reported[12] that laminated devices may impose additional mechanical compression that shrink the pores or otherwise change their supramolecular structure.

Multilayer paper design

Next, the effect of multiple layers of paper on the flow rate was investigated. Since 1710, various mathematical fits to model flow between closely positioned substrates (glass capillaries, paper, *etc.*) have been reported.[44–51] However, the application of fast flow between paper layers has received comparatively little attention. Recently, parallel substrates (hydrophilic and hydrophobic) have been used in tandem for fast and continuous flow for applications in paper spray ionization.[52] Previous reports on fast flow μPADs have employed 2 layers of paper or hollow channels.[9,10,18] In this study, the flow rate of 150 μL of red dye down the length of the device (6.22 cm) was noticeably faster for 2- (0.010 cm s^{-1}) and 3- (0.0075 cm s^{-1}) layer devices compared to 1- (0.0047 cm s^{-1}) layer devices as shown in Fig. 2b. This is attributed to the generation of ~12 μm gaps or channels between the paper layers upon wetting, as has been previously observed.[9,10] Interestingly, μPADs with 3 layers of paper reproducibly exhibited slower flow rates than those with 2 layers. To the best of our knowledge, μPADs featuring 3 or more layers have not been previously investigated quantitatively. We hypothesize the slower flow rate in the 3-layer device is due to swelling of the paper fibers between the tape, compressing the paper layers together and thereby reducing the effective channel heights between the layers (*i.e.* the distance between the 2 paper layers).[9] Whereas in the 2-layer device, the paper swells against the tape leaving the channel the same height or greater as previously observed.[9] This effect is illustrated in Fig. S1 (ESI†).

To probe this non-uniform swelling hypothesis, 2-layer μPADs were fabricated with and without a 1 layer of 78 μm thick double-sided tape between the paper layers (ESI† Fig. S2, Fig. 1a-iii). Devices without tape exhibited faster flow rates (0.035 *vs.* 0.023 cm s^{-1}) but showed larger variability (39% *vs.* 15% relative standard deviation) in the flow rate (ESI† Fig. S2, flow rate calculated as time required to trans-verse 5.55 cm). As hypothesized, the faster yet more variable flow is likely due to variations in the layer separation and manual device fabrication of each device.[9] Therefore, the use of double sided tape was investigated as a means to tune the flow rates in multilayer μPADs through control of the channel height.

†Electronic supplementary information (ESI) available: Fig. S1–S7 investigate the swelling in 2 and 3 layer μPADs, the velocity in multilayer μPADs with and without double sided sticky tape between the layers, with different orientations, with different paper types and with different volumes. Channel heights are estimated based on these velocities, and snapshot photographs of a multilayered 3DPN during sequential injection of $FcTMA^+$ are provided. See DOI: 10.1039/c7lc01300k

Effect of channel height and device orientation on flow rates in multilayer μPADs

Straight channel μPADs with 2 layers of paper were designed featuring different numbers of double sided tape layers (each layer added 78 μm) between the paper layers to investigate the effect of channel height on flow rate. Theoretical flow rates for multilayer μPADs have previously been treated through eqn (1), using a modified term for the effective pore radius developed by *Martinez et al.*,[10]

$$r = \frac{2r'(hw) + R(gw)}{2hw + gw} \quad (2)$$

where r' is mean capillary radius of the paper, h is the paper thickness, w is the channel width, g is the channel height (distance between the paper layers) and $R = g/2$ is the half channel height, with all measurements in meters. Eqn (2) treats the distance between the layers as a row of large circular pores of radius R.

Upon increasing the channel height, the flow rate increases as expected from eqn (1) and (2) (Fig. 3a). However, we observe a maximum in the flow rate with a 234 μm channel height (3 layers of tape), after which the flow rate decreases for increasing channel heights. This phenomenon is contrary to predictions that anticipate increased flow rates with increased pore radii (eqn (2)). However, these devices were initially investigated by holding the μPADs vertically (with the channel perpendicular to the workbench), and lowering them into sample wells. Therefore, we attribute this result to the opposing forces of gravity acting on the sample mass and capillary action driven by the hydrophilic paper walls; for large channel heights, the benefit of increased pore radii is offset by the body force. To test this hypothesis, the experiment was repeated with the μPADs positioned horizontally (*i.e.* parallel the workbench, orthogonal to gravity). As shown in Fig. 3b, the horizontal orientation leads to a dramatic increase in flow rate, particularly for large channel height devices. A video showing device operation is provided as ESI † In fact, the velocity in horizontal devices with a 390 μm channel height (5 layers of tape) represents a 58× increase (1.56 ± 0.30 cm s^{-1}) over vertical multilayer devices with the same channel height (0.027 ± 0.002 cm s^{-1}), and a remarkable 145× increase over 1-layer μPADs (0.011 ± 0.001 cm s^{-1}) for flow over 5.55 cm.

Analytical treatments of multilayer flow μPADs

Prediction of the observed flow rates using eqn (1) and (2) proved unreliable, with a large discrepancy between the predicted and experimental flow rates. The theoretical velocity and volumetric flow rate for the fastest device (5 layers of tape, 390 μm channel height, horizontally orientated, velocity and volumetric flow rates are averaged over 6.55 cm device length) are 8.57 cm s^{-1} and 9.06 mL min^{-1} respectively based on eqn (1) and (2). These are significantly faster than our experimental values (1.85 cm s^{-1} or 1.95 mL min^{-1}) over the same distance and faster than any flow rates previously reported in μPADs. In fact, based on the observed flow rates, these equations predict significantly smaller channel heights than are present in the devices (ESI,† Fig. S3, *e.g.*, 234 μm fabricated height *versus* 39.7 μm calculated). However, eqn (2) was developed for multilayer μPADs with small channel heights (~12 μm).[9,10] This suggests the source of the rapid flow is more complicated than the presence of large pores between the layers as predicted by Lucas–Washburn flow.

Aside from capillary action, the main factors that could influence the fluid flow in μPADs are gravity, evaporation, pressure-driven flow, and head pressure from the inlet solution. The devices tested within this study are sealed in tape and previous investigations have shown evaporation to be minimal in sealed devices at typical laboratory humidity ranges (25 to 40%).[9] Pressure-driven flow could be caused by head pressure as a result of differences in liquid levels at the device inlet and is characterized by a convex (parabolic) fluid front. Conversely, flow driven by capillary action exhibits a concave fluid front. Therefore, a multilayered μPAD (390 μm channel height), was imaged normal to the direction of fluid flow, during flow of a red colored dye (Fig. 4). For both vertical and horizontal devices (Fig. 4), a concave fluid front is observed, suggesting head pressure is not the dominant driving force for either orientation. Interestingly, the flow profile is concave across the channel height but convex across the channel width (parallel to the paper). To confirm that gravity is the main cause of the disparity between flow in different device orientations, the change in flow velocity was measured for μPADs held horizontally (red squares), vertically (blue circles) and at a 45° angle (green triangles), (Fig. 5). Interestingly, the velocities are similar over short distances (within one standard deviation for <2 cm traversed), but diverge dramatically over longer distances. A similar trend is observed for orientation experiments in μPADs using 1 layer of paper, although the divergence between the orientations is significantly smaller (ESI† Fig. S4). These data are in accordance with the hypothesis that gravity retards flow in vertically orientated μPADs, and that this effect is pronounced in multilayer devices.

There are a few literature examples of fast flow μPADs employing different channel formation concepts using either microchannels (150 μm by 50 μm) mechanically cut into the paper,[15,16] multilayers with unfixed height (12 μm by 5 mm),[9] hollow channels between wax and paper (180 μm by 2.5 mm),[18,22] or hollow channels between PDMS and paper (160 μm by 1 mm).[53] Unfortunately, the exact mechanism of fast flow in these examples are rarely discussed, though the addition of external forces such as head pressure or syringe pumps are likely a major driving force. To set our fast flow rates in context, Table 1 provides velocities and volumetric flow rates for literature examples of fast flow μPADs. These values illustrate the different approaches but do not reflect optimal speeds due to different priorities and levels of optimization in the different studies, as well as different device channel lengths and widths. For example, the velocity for the 5 layers of tape device (horizontal) is 15.5 and 5.09 cm s^{-1} over 1.55 and 3.55 cm respectively. Note, these alternate methods do not achieve the same velocities and/or volumetric flow rates as the multilayer μPADs, even with the use of more expensive or complex approaches such as using syringe pumps or inlet wells to create pressure-driven flow.

Effect of paper type and sample volume on flow rates

Different paper types were also tested with 3DPNs (3 layers of tape, 234 μm channel height, held horizontally), as the paper thickness and porosity are known to affect the flow rate.[55] However, as shown in Table 2 (and ESI† Fig. S5), after taking account of pore sizes and paper thicknesses, no significant change was seen in the flow rate based on an unpaired *t*-test at 95% confidence interval ($n = 5$ for each paper type). This further supports the hypothesis

that the flow between the paper layers is the dominant driving force for the rapid flow rates in these μPADs, rather than flow in the paper alone.

Aside from selecting the best substrate, the optimal sample volume for a device is not often discussed. Eqn (1) and (2) assume an infinite sample volume,[5] which is rarely applicable to real systems. Practically, sample volume is either finite and controlled (*e.g.*, optimized analytical assays)[34] or an uncontrolled amount exceeding the device capacity (*e.g.*, the pregnancy test). Therefore, the effect of sample volume on the flow rate for vertically orientated 1- and 2-layer μPADs was investigated. As shown in Fig. 6, two velocity regimes are evident; while there is liquid within the sample inlet, a Lucas–Washburn type exponential decay in the velocity is observed (black dashed curved line). After the inlet sample is drained, the flow rate abruptly switches to a second slower re gime (red, blue and grey dashed lines) likely the result of slow wetting of the paper fibers above the bulk liquid, coupled with surface tension. A picture of the device showing the final positions of the fluid fronts for the different volumes is provided in the ESI† (Fig. S6).

The effect of the sample volume in a 1 layer of paper device was also investigated using 10, 20, 40, 60, and 80 μL of blue food dye (ESI† Fig. S6). As expected, devices with larger volumes exhibited faster flow and longer distances traveled. However, over several experiments the 60 μL test consistently showed faster flow than 80 μL and 200 μL tests. We attribute this phenomenon to greater intermolecular forces such as hydrogen bonding in larger sample volumes. As shown in ESI† Fig. S6, with an excess of sample in the reservoir, the cohesive properties of water (solvent) act in opposition to the capillary forces of the paper. This is not observed in the 2-layer devices, likely the result of larger capillary forces able to overcome these intermolecular forces. Further studies are underway to investigate if this phenomenon is observed in 2-r devices at larger sample volumes. Based on these results, we envision sample volume is another factor that can be manipulated for controlling the flow rate in 3DPNs. For example, fast staged flow with a slow intermediate step could be carried out through addition of multiple aliquots, for assay steps that require slow reactions.[14,24]

Development of a sequential-injection 3DPN device

As previously discussed, the controlled addition of reagents in an assay is an important challenge to the μPAD field. Here, we applied the concepts from the multilayer paper device to design a 3DNP device (Fig. 7a). The device design is similar to that developed by Fu/Lutz/Yager and coworkers.[30,33,34,56] When aliquots are added to the sample inlet legs (Fig. 7a-ii circles), the liquids reach the main channel, then deplete sequentially.[19] A 270° fan geometry is placed at the end of the μPAD channel to ensure generation of a constant flow rate and complete depletion of sample in the inlet wells.[8,9] Microwire electrodes (Fig. 7a-iv) are placed across the channel, normal to the direction of flow, positioned in between the bottom layer of wax modified paper (Fig. 7a-ii) and the double sided tape (Fig. 7a-iii). To characterize these devices, a flow injection analysis (FIA) experiment was performed using $FcTMA^+$ in 1-layer μPAD and 3DPN devices. To initiate flow, 80 μL aliquots of a) KNO_3, b) 1 mM $FcTMA^+$ with 0.1 M KNO_3 spiked with a yellow dye, and finally c) 0.1 M KNO_3 spiked with a green dye were added to the sample wells (right to left, *i.e.* KNO_3 first). Dyes were used to visually confirm solution mixing but did not contribute to Faradaic signals.

As shown in Fig. 7b, there is a dramatic reduction in the residence time (time between injection and maximum signal) from 1025 s to 363 s on switching from a 3DPN device with 1 layer of paper (blue line) to two. A further reduction to 17 s is observed on increasing the channel height from 1 layer thickness of tape (black line, channel height = 78 μm) to 3 layers of tape (orange line, channel height = 234 μm). The chronoamperometric profile in the 1-layer and smaller channel height devices (blue and black) are typical of classical FIA experiments, featuring an asymmetrical peak with a long tailed current decay back to baseline. Larger peak currents are observed in the multilayer devices due to the greater flow rate, which, in turn increases mass transport to the electrode surface. The FIA profiles feature some dispersion indicators, such as the slow initial increase in current for the 1 layer of tape 3DPN (black line). This dispersion can be observed visually from images of this device during flow, which are provided in the supporting information (ESI† Fig. S7). The smaller currents observed in the multilayer 3DPN with 3 layers of tape (orange line) over the 1 layer of tape device (black line) indicate that dispersion is more prevalent in larger-channel devices, however further device optimization and design should allow a reduction in this effect and is the subject of ongoing work.

The estimated velocities during the $FcTMA^+$ injections were 0.98, 0.030 and 0.010 cm s^{-1}, respectively, for the 3 and 1 layers of tape 3DPN and 1 layer of paper devices. These values coupled with the peak currents suggest that the smaller channel height device gives higher collection efficiency as predicted from previously published models of microwire electrochemistry in classical flow cells.[57] Conversely, a significant proportion of the analyte likely flows past the electrode without being oxidized with larger channel heights. The peak currents in both cases are reasonable based on the estimated flow rates, however the experimental currents could not be fit to this model.[57] We hypothesize this is due to the significantly different flow profiles in these multilayer μPADs compared to classical Poiseuille flow in syringe pump driven flow devices. This problem should be treatable through computational modeling of the fluid dynamics, and would allow further optimization of these 3DPN devices. This subject is under currently under investigation. Importantly, the total time for sequential injection in the 3 layers of tape 3DPN μPAD is ~1 min, which compares favorably with previous sequential injection μPAD designs based around 1 layer of paper (~3,[23] 6,[33] 8,[17] 9,[56] 15,[34] and 60 min (ref. 30)).

Application of the 3DPN for the stripping analysis of cadmium

Sequential injection μPADs have been applied previously for colorimetric reactions with dyes,[19,56] involving pH changes,[34] immunoassays of malaria antigens,[30] or pesticide sensors.[17] However, they are yet to be demonstrated for electrochemical reactions. Here we demonstrate the 3DPN device scope for the square-wave anodic stripping analysis of cadmium. Cadmium exposure is linked to kidney failure, skeletal damage and cancer.[58] Therefore, POC detection methods, especially for particulate matter and waste water matrices are of significant importance.[59,60] Our approach is adapted from a previously reported method where bismuth is used to facilitate adsorption of the cadmium onto a silver electrode.[60] Sequential injections of 640 μg L^{-1} bismuth in acetate buffer (40 μL), 400 μg L^{-1} cadmium in acetate buffer (80 μL), and acetate buffer only (pH 5, 80 μL) were applied to different μPADs as shown in Fig. 8. A deposition potential of −1.6 V is applied during the

bismuth and cadmium injection, and square-wave stripping is carried out during the final injection (visualized through addition of non-electroactive dyes to the injections).

For pulsed voltammetry techniques, the peak area is known to be a better indicator of concentration than peak current due to the commonly observed shifting potential of peaks and variability of the background currents.[61] There is a clear increase in the peak area (3.5×) and thus sensitivity when moving from spot test (green) to the flowing μPADs. Additionally, moving from a 1-layer μPAD (blue) to a 3DPN (2 layers of paper, black) with 1 layer of tape and a 3DPN with 3 layers of tape (orange) evoke 1.37× and 1.43× increases in the peak area. We attribute this greater signal in the microfluidic devices compared to the spot test to the increased convective pre-concentration of the bismuth and cadmium onto the microwire electrode. The signal increases from spot test to μPAD, and tailing off of signal enhancement for faster flow (larger channel height) 3DPN can be rationalized as follows: In the spot test, a deposition time of 360 s used, whereas in the μPADs the deposition time is based upon the time taken for the first two injections to traverse the electrodes. Therefore, deposition times of for the 1 layer of paper, 3DPN (1 layer of tape) and 3DPN (3 layers of tape) devices respectively. During injection, some material is left in the inlet legs, therefore not all 80 μL will be transported to the electrodes (ESI† Fig. s7-e). This effect is likely exacerbated for multilayer devices with large channel heights and, thus, more material trapped in the inlet legs between the layers. Depending on the mass transport and fluid mixing between injections, some of the material likely passes the electrodes without being oxidized for the fastest flow rate 3DPN. Ongoing work seeks to optimize these devices through additional modeling and characterization of the flow in these multilayer devices.

Conclusions

Herein, 2-layer μPADs with controlled channel heights have been demonstrated featuring substantially faster flow rates than previously described μPAD designs without flow-rate enhancement methods (such as syringe pumps or head pressure to drive flow). Through our investigations we have ob served that rapid flow rates are possible with multi-layered devices using large channel heights (100–400 μm), where the height is simply controlled through addition of double sided tape along the channel edge. Velocities and volumetric flow rates of 3.71 cm s^{-1} (3.92 mL min^{-1}) and 1.34 cm s^{-1} (1.41 mL min^{-1}), were observed for flow over the first 1.55 and 6.55 cm respectively in a horizontally oriented μPAD (390 μm channel height).

Interestingly, the flow rates do not fit established models of flow within μPADs and analytical and computational treatment of flow within these devices is the subject of ongoing work. The effect of orientation (gravity), channel height, sample volume and paper type are investigated, and compared to classical μPAD designs. These multilayer μPADs have increased the flow rate over two orders of magnitude compared to 1-layer μPADs over long channel lengths (6.55 cm), without the need for external pumps, mechanical intervention, or external signals (*e.g.*, dielectric switches) with good control.[14] These insights are also applied to a sequential injection 3DPN device, for the flow injection analysis of $FcTMA^+$ and the stripping voltammetry of cadmium. From the rapid injection time, short residence

time, and enhanced sensitivity (5×) compared to stationary PADs, 3DPN should be applicable for a wide range of analytes and point-of-care applications.

We envision the flow rates in μPADs could be further enhanced through addition of inlet sample volume (pressure-driven flow),[18,22] optimization of the slip angle,[17] or control of the channel width or length.[23,62] Full characterization of the flow profile within these multilayer μPADs would allow for placement of microwires in regions of highest velocity within the cross section. This should enhance the mass transport and increase the device sensitivity compared to classical microfluidic devices with electrodes carefully entrenched into the channel walls.[9,22,63,64] Furthermore, this 2-layer format should allow for the optimized transport and detection of larger species such as micron-sized particles,[65] and blood cells in μPADs,[28] through the increased channel height.

Supplementary Material

Refer to Web version on PubMed Central for supplementary material.

Acknowledgements

RBC, JV, and CSH thank the National Institute of Occupational Safety and Health (OH010662) for project support. Additional support was provided through NSF (1537486). We thank Dr. J. Adkins and J. Nejad (CSU) for helpful discussions on μPAD literature and fluid dynamics respectively.

References

1. Vashist SK, Luppa PB, Yeo LY, Ozcan A and Luong JHT, Trends Biotechnol, 2015, 33, 692–705. [PubMed: 26463722]
2. St John A and Price CP, Clin. Biochem. Rev, 2014, 35, 155–167. [PubMed: 25336761]
3. Shafiee H, Wang S, Inci F, Toy M, Henrich TJ, Kuritzkes DR and Demirci U, Annu. Rev. Med, 2015, 66, 387–405. [PubMed: 25423597]
4. Yetisen AK, Akram MS and Lowe CR, Lab Chip, 2013, 13, 2210–2251. [PubMed: 23652632]
5. Cate DM, Adkins JA, Mettakoonpitak J and Henry CS, Anal. Chem, 2015, 87, 19–41. [PubMed: 25375292]
6. Yang Y, Noviana E, Nguyen MP, Geiss BJ, Dandy DS and Henry CS, Anal. Chem, 2017, 89, 71–91. [PubMed: 27936612]
7. Yamada K, Henares TG, Suzuki K and Citterio D, Angew. Chem., Int. Ed, 2015, 54, 5294–5310.
8. Mendez S, Fenton EM, Gallegos GR, Petsev DN, Sibbett SS, Stone HA, Zhang Y and López GP, Langmuir, 2010, 26, 1380–1385. [PubMed: 19845342]
9. Adkins JA, Noviana E and Henry CS, Anal. Chem, 2016, 88, 10639–10647. [PubMed: 27749031]
10. Camplisson CK, Schilling KM, Pedrotti WL, Stone HA and Martinez AW, Lab Chip, 2015, 15, 4461–4466. [PubMed: 26477676]
11. Gong MM, Nosrati R, San Gabriel MC, Zini A and Sinton D, J. Am. Chem. Soc, 2015, 137, 13913–13919. [PubMed: 26447553]
12. Nguyen MP, Meredith NA, Kelly SP and Henry CS, Lab Chip, 2018, DOI: 10.1016/j.aca.2018.01.036.
13. Wang CC, Hennek JW, Ainla A, Kumar AA, Lan WJ, Im J, Smith BS, Zhao M and Whitesides GM, Anal. Chem, 2016, 88, 6326–6333. [PubMed: 27243791]
14. Fu E and Downs C, Lab Chip, 2017, 17, 614–628. [PubMed: 28119982]
15. Giokas DL, Tsogas GZ and Vlessidis AG, Anal. Chem, 2014, 86, 6202–6207. [PubMed: 24915155]

16. Glavan AC, Martinez RV, Maxwell EJ, Subramaniam AB, Nunes RMD, Soh S and Whitesides GM, Lab Chip, 2013, 13, 2922–2930. [PubMed: 23719764]
17. Jahanshahi-Anbuhi S, Chavan P, Sicard C, Leung V, Hossain SMZ, Pelton R, Brennan JD and Filipe CDM, Lab Chip, 2012, 12, 5079–5085. [PubMed: 23079674]
18. Renault C, Li X, Fosdick SE and Crooks RM, Anal. Chem, 2013, 85, 7976–7979. [PubMed: 23931456]
19. Dharmaraja S, Lafleur L, Byrnes S, Kauffman P, Buser J, Toley B, Fu E, Yager P and Lutz B, Proc. SPIE, 2013, 86150X.
20. Castro C, Rosillo C and Tsutsui H, Microfluid. Nanofluid, 2017, 21, 21.
21. Berli CLA and Kler PA, Microfluid. Nanofluid, 2016, 20, 104.
22. Renault C, Anderson MJ and Crooks RM, J. Am. Chem. Soc, 2014, 136, 4616–4623. [PubMed: 24635569]
23. Songok J and Toivakka M, Microfluid. Nanofluid, 2016, 20, 63.
24. Schonhorn JE, Fernandes SC, Rajaratnam A, Deraney RN, Rolland JP and Mace CR, Lab Chip, 2014, 14, 4653–4658. [PubMed: 25300302]
25. Bathany C, Han J-R, Abi-Samra K, Takayama S and Cho Y-K, Biosens. Bioelectron, 2015, 70, 115–121. [PubMed: 25797850]
26. Santhiago M, Bettini J, Araújo SR and Bufon CCB, ACS Appl. Mater. Interfaces, 2016, 8, 10661–10664. [PubMed: 27065112]
27. Schilling KM, Lepore AL, Kurian JA and Martinez AW, Anal. Chem, 2012, 84, 1579–1585. [PubMed: 22229653]
28. Fernandes SC, Walz JA, Wilson DJ, Brooks JC and Mace CR, Anal. Chem, 2017, 89, 5654–5664. [PubMed: 28406607]
29. Gong MM and Sinton D, Chem. Rev, 2017, 117, 8447–8480. [PubMed: 28627178]
30. Fridley GE, Le H and Yager P, Anal. Chem, 2014, 86, 6447–6453. [PubMed: 24882058]
31. Cate DM, Noblitt SD, Volckens J and Henry CS, Lab Chip, 2015, 15, 2808–2818. [PubMed: 26009988]
32. Apilux A, Ukita Y, Chikae M, Chailapakul O and Takamura Y, Lab Chip, 2013, 13, 126–135. [PubMed: 23165591]
33. Fu E, Kauffman P, Lutz B and Yager P, Sens. Actuators, B, 2010, 149, 325–328.
34. Fu E, Lutz B, Kauffman P and Yager P, Lab Chip, 2010, 10, 918–920. [PubMed: 20300678]
35. Han KN, Choi J-S and Kwon J, Sci. Rep, 2016, 6, 25710. [PubMed: 27174731]
36. Gerbers R, Foellscher W, Chen H, Anagnostopoulos C and Faghri M, Lab Chip, 2014, 14, 4042–4049. [PubMed: 25155271]
37. Liu W, Cassano CL, Xu X and Fan ZH, Anal. Chem, 2013, 85, 10270–10276. [PubMed: 24117197]
38. Liu F and Zhang C, Sens. Actuators, B, 2015, 209, 399–406.
39. Schoelkopf J, Gane PAC, Ridgway CJ and Matthews GP, Colloids Surf., A, 2002, 206, 445–454.
40. Lemay SG, van den Broek DM, Storm AJ, Krapf D, Smeets RMM, Heering HA and Dekker C, Anal. Chem, 2005, 77, 1911–1915. [PubMed: 15762604]
41. Fischer LM, Tenje M, Heiskanen AR, Masuda N, Castillo J, Bentien A, Émneus J, Jakobsen MH and Boisen A, Microelectron. Eng, 2009, 86, 1282–1285.
42. Polk BJ, Stelzenmuller A, Mijares G, MacCrehan W and Gaitan M, Sens. Actuators, B, 2006, 114, 239–247.
43. da Silva ETSG, Santhiago M, de Souza FR, Coltro WKT and Kubota LT, Lab Chip, 2015, 15, 1651–1655. [PubMed: 25686364]
44. Taylor B, Philos. Trans. R. Soc. London, 1710, 27, 538.
45. Hauksbee F, Philos. Trans. R. Soc. London, 1710, 27, 539–540.
46. Jurin J, Philos. Trans. R. Soc. London, 1717, 30, 739–747.
47. de Laplace PS, Traité de mécanique céleste, Chez J.B.M. Duprat, 1805.
48. Young T, Peacock G and Leitch J, Miscellaneous works of the late Thomas Young, ed. Murray J, 1855.

49. Fujita H, J. Phys. Chem, 1952, 56, 625–629.
50. Higuera FJ, Medina A and Liñán A, Phys. Fluids, 2008, 20, 102102.
51. Luo C, Heng X and Xiang M, Langmuir, 2014, 30, 8373–8380. [PubMed: 24979670]
52. Salentijn GIJ, Permentier HP and Verpoorte E, Anal. Chem, 2014, 86, 11657–11665. [PubMed: 25409532]
53. Ravi Kumar A, Nivedita P, Kaustav C, Nripen C, Gautam B and Suman C, J. Micromech. Microeng, 2016, 26, 105008.
54. Shin J-H, Lee G-J, Kim W and Choi S, Sens. Actuators, B, 2016, 230, 380–387.
55. Evans E, Gabriel EFM, Coltro WKT and Garcia CD, Analyst, 2014, 139, 2127–2132. [PubMed: 24618915]
56. Fu E, Ramsey SA, Kauffman P, Lutz B and Yager P, Microfluid. Nanofluid, 2011, 10, 29–35. [PubMed: 22140373]
57. Fulian Q, Gooch KA, Fisher AC, Stevens NP and Compton RG, Anal. Chem, 2000, 72, 3480–3485. [PubMed: 10952531]
58. Järup L, Br. Med. Bull, 2003, 68, 167–182. [PubMed: 14757716]
59. Martín-Yerga D, Álvarez-Martos I, Blanco-López MC, Henry CS and Fernández-Abedul MT, Anal. Chim. Acta, 2017, 981, 24–33. [PubMed: 28693726]
60. Mettakoonpitak J, Mehaffy J, Volckens J and Henry CS, Electroanalysis, 2017, 29, 880–889.
61. Monk PMS, Fundamentals of Electro-Analytical Chemistry, Wiley, 2008.
62. Hong S and Kim W, Microfluid. Nanofluid, 2015, 19, 845–853.
63. Růžička J and Hansen EH, Flow Injection Analysis, Wiley J, New York, 2nd edn, 1988.
64. Fosdick SE, Anderson MJ, Renault C, DeGregory PR, Loussaert JA and Crooks RM, Anal. Chem, 2014, 86, 3659–3666. [PubMed: 24625315]
65. Cunningham JC, Kogan MR, Tsai Y-J, Luo L, Richards I and Crooks RM, ACS Sens, 2016, 1, 40–47.

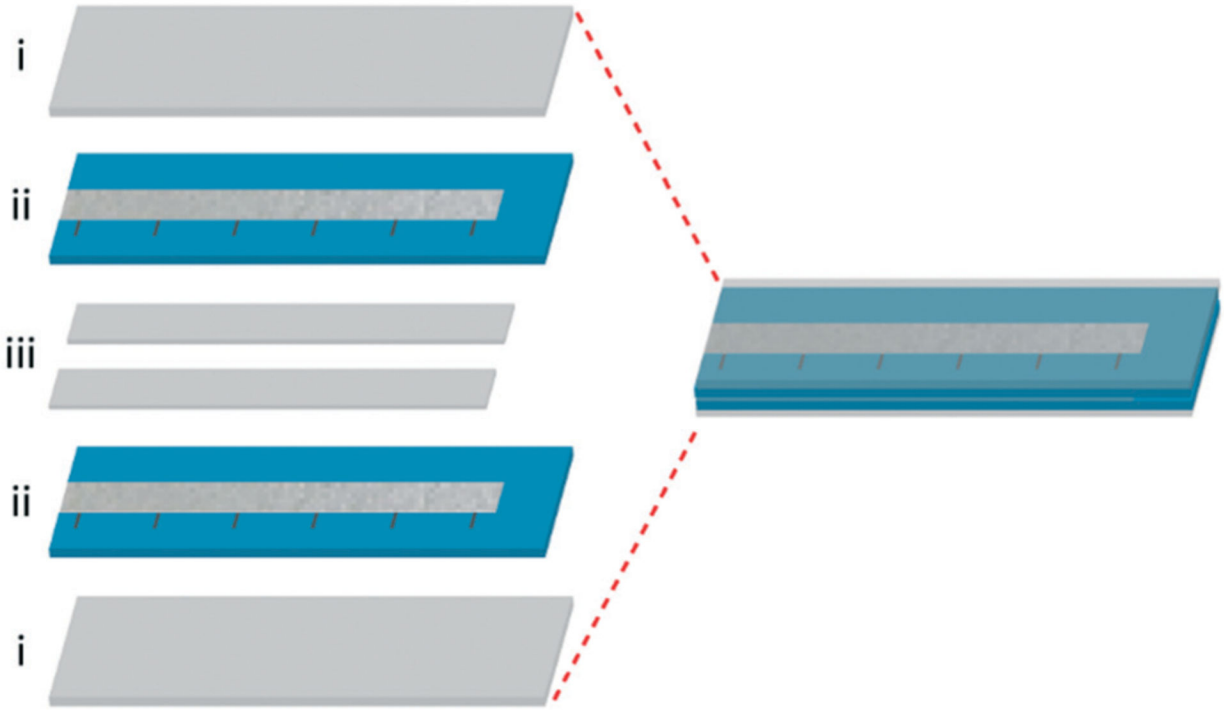

Fig. 1.

Illustration of straight channel multilayer μPADs, fabricated from i) packing tape, ii) wax-modified Whatman 1 qualitative paper and iii) double sided tape.

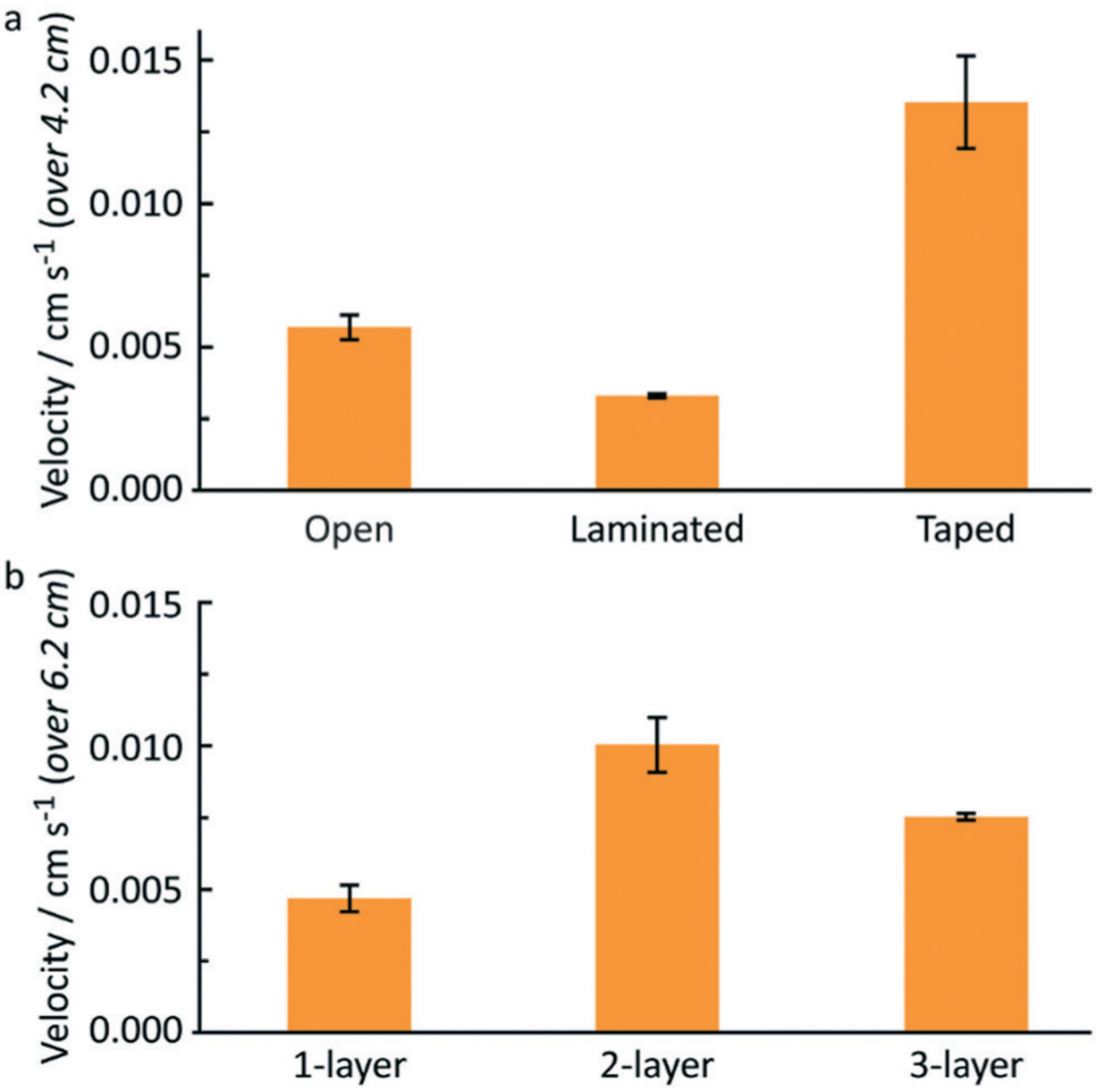

Fig. 2.

a) Open, laminated and taped sealing for straight channel μPADs, average velocity over 4.2 cm, b) taped μPADs with different numbers of paper layers, average velocity over 6.2 cm, with 150 μL aliquot of red dye, error bars represent the standard deviation ($n = 5$), these devices were oriented vertically.

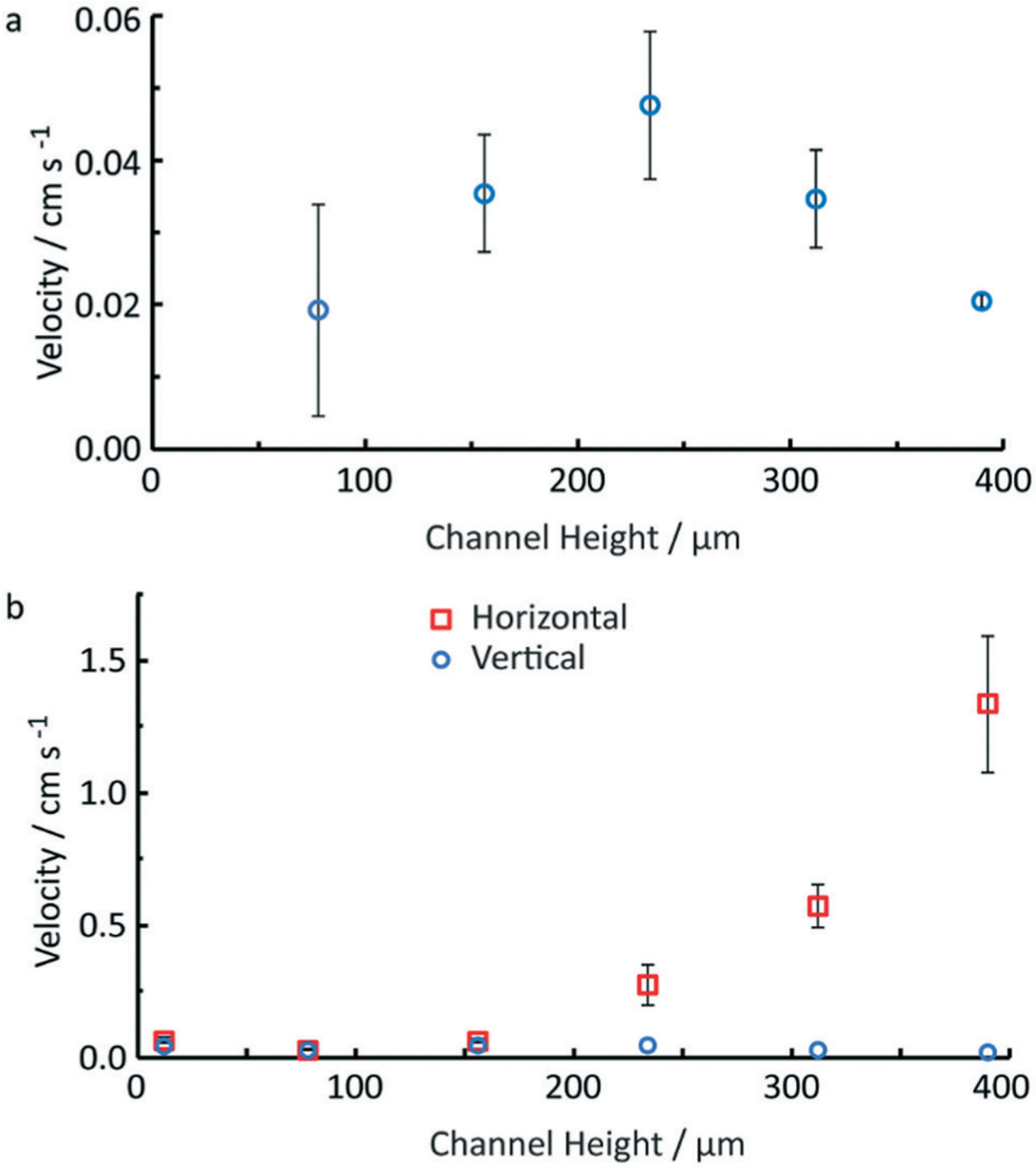

Fig. 3.

Effect of channel height on flow rate for a) vertical (blue circles) and b) horizontal (red squares) 2-layer µPADs, error bars represent the standard deviation ($n = 5$). Note, these flow rates are calculated based on the time taken for colored dye to flow 6.55 cm down a straight channel µPAD.

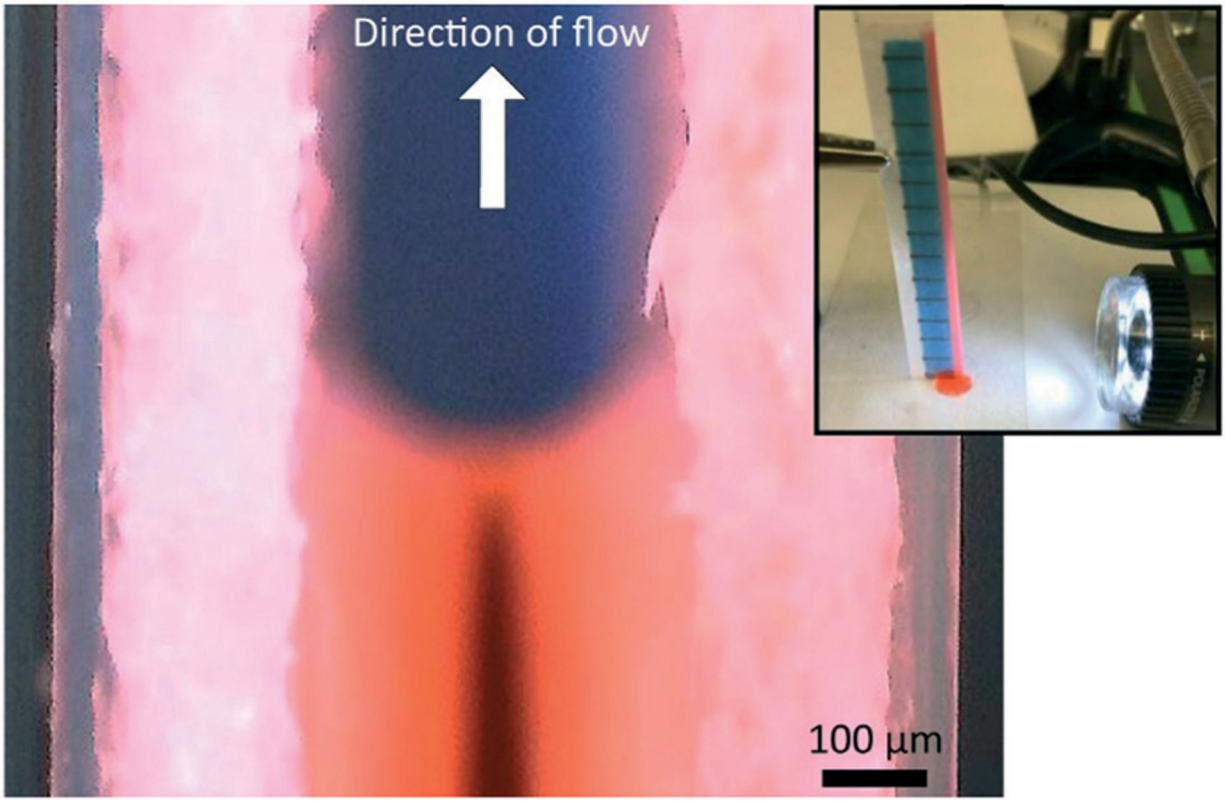

Fig. 4.

Photograph of flow for a red dye within a multilayered µPAD (390 µm channel height *i.e.* 5 layers of tape) orientated vertically. Devices viewed normal to the direction of flow, as shown in the inset.

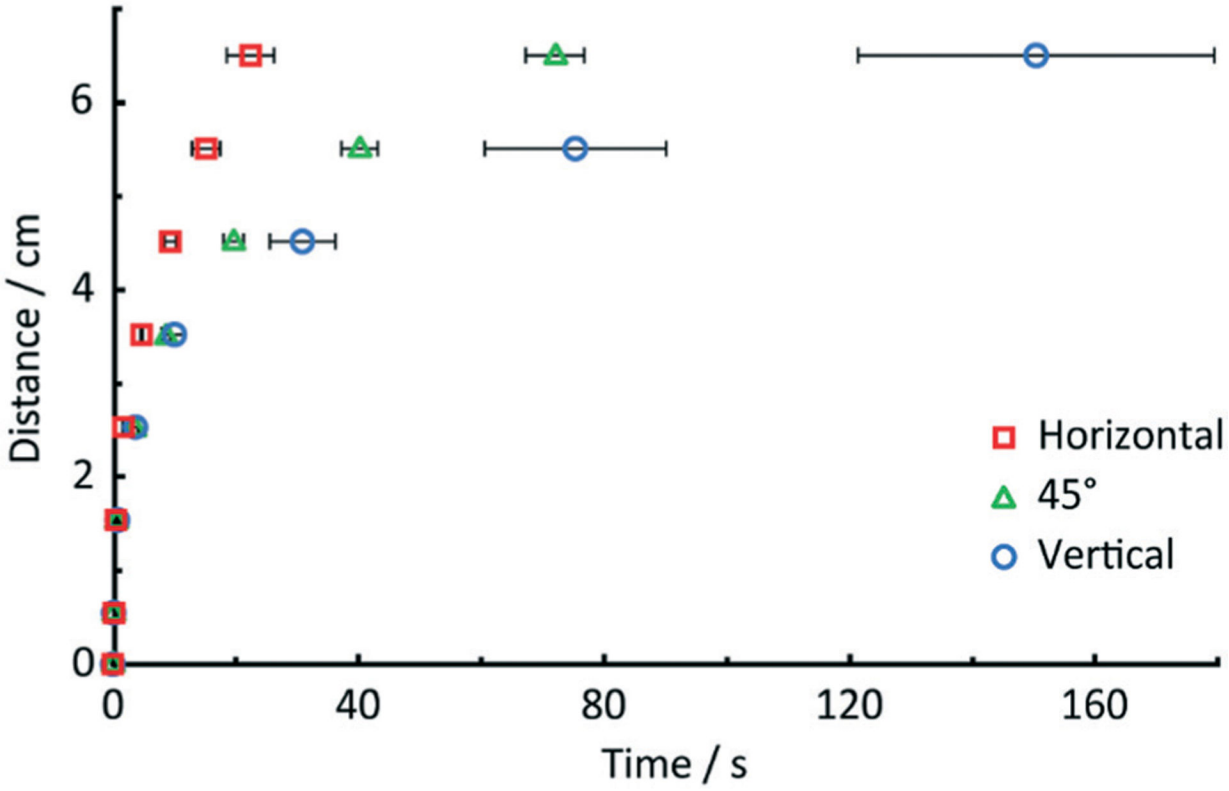

Fig. 5.

Length traversed down straight channel 2-layer μPADs with 234 μm channel height, for horizontal (0°), 45° and vertical (90°) placement above the workbench, error bars represent the standard deviation ($n = 5$).

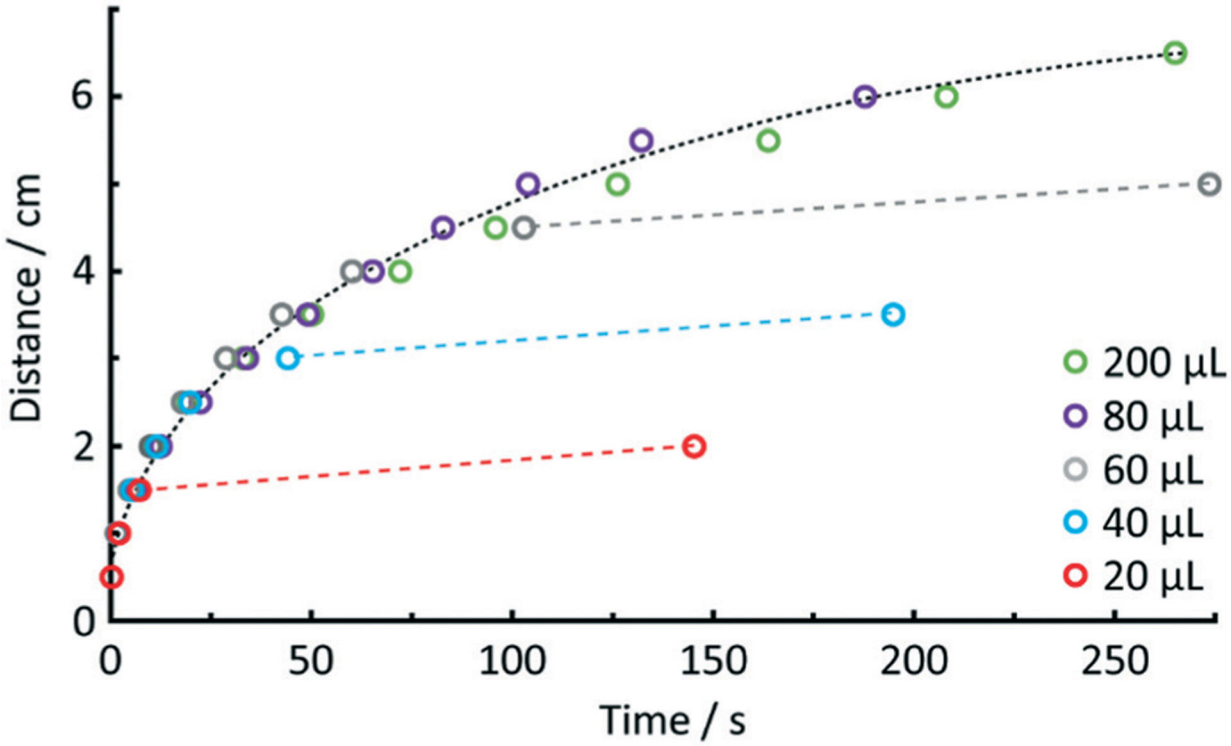

Fig. 6.

Effect of sample volume on flow rate for straight channel 2-layer µPADs with 234 µm channel height (vertical, $n = 5$). Dashed lines represent best-fit approximations to illustrate the primary flow regime (black dashed curve) and the secondary flow regime upon depletion of the inlet wells (red, blue and grey dashed lines).

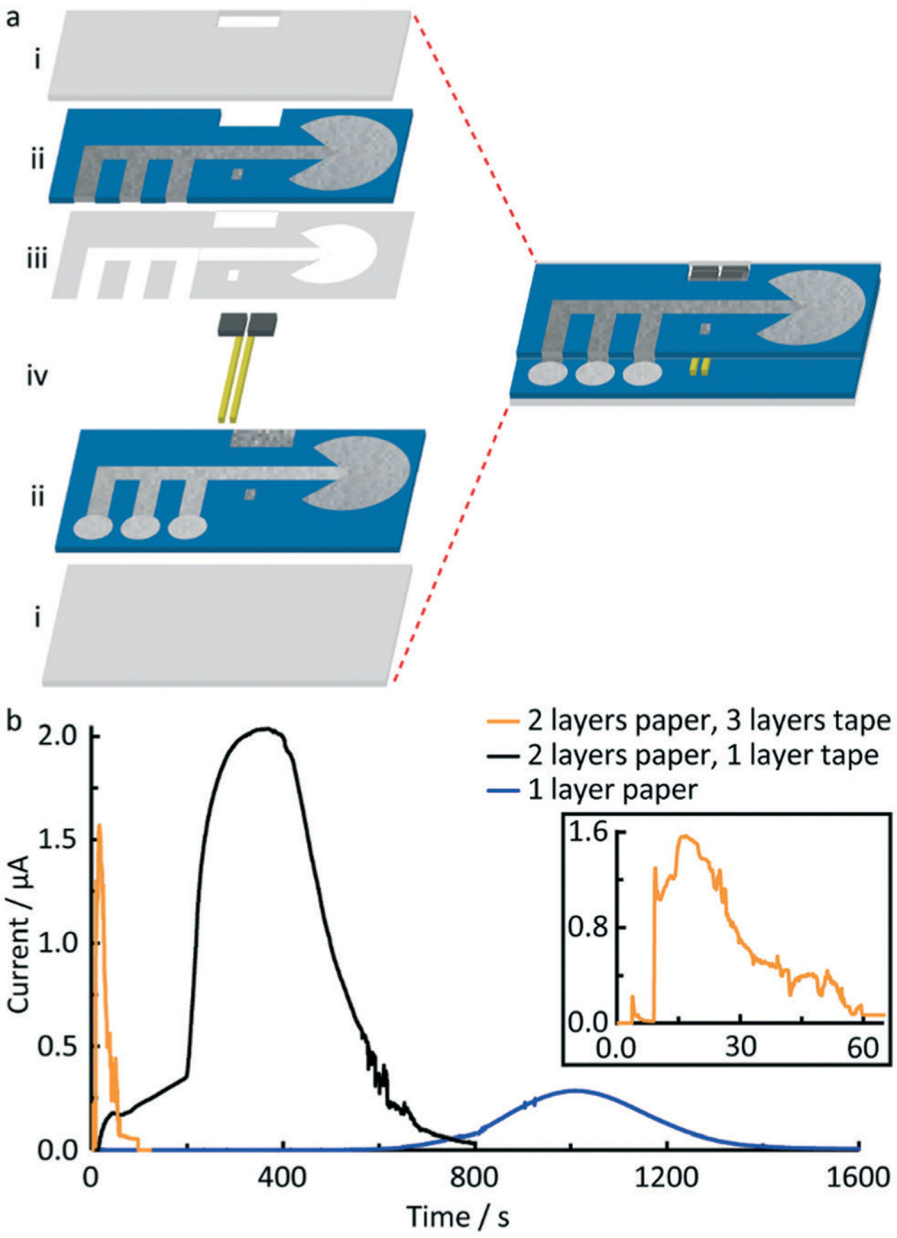

Fig. 7.

a) Illustration 3DPNs, fabricated from i) packing tape, ii) wax-modified Whatman 1 qualitative paper, iii) double sided tape, and iv) microwire electrodes. b) Flow injection analysis with 80 µL of 1 mM $FcTMA^+$ in 0.1 M KNO_3 using 3DPN devices with 1 layer of paper (blue), 2 layers of paper with 1 layer of tape (black), and 2 layers of paper with 3 layers of tape between the layers (orange, on main plot and inset), potential = 0.5 V *vs.* Ag/AgCl.

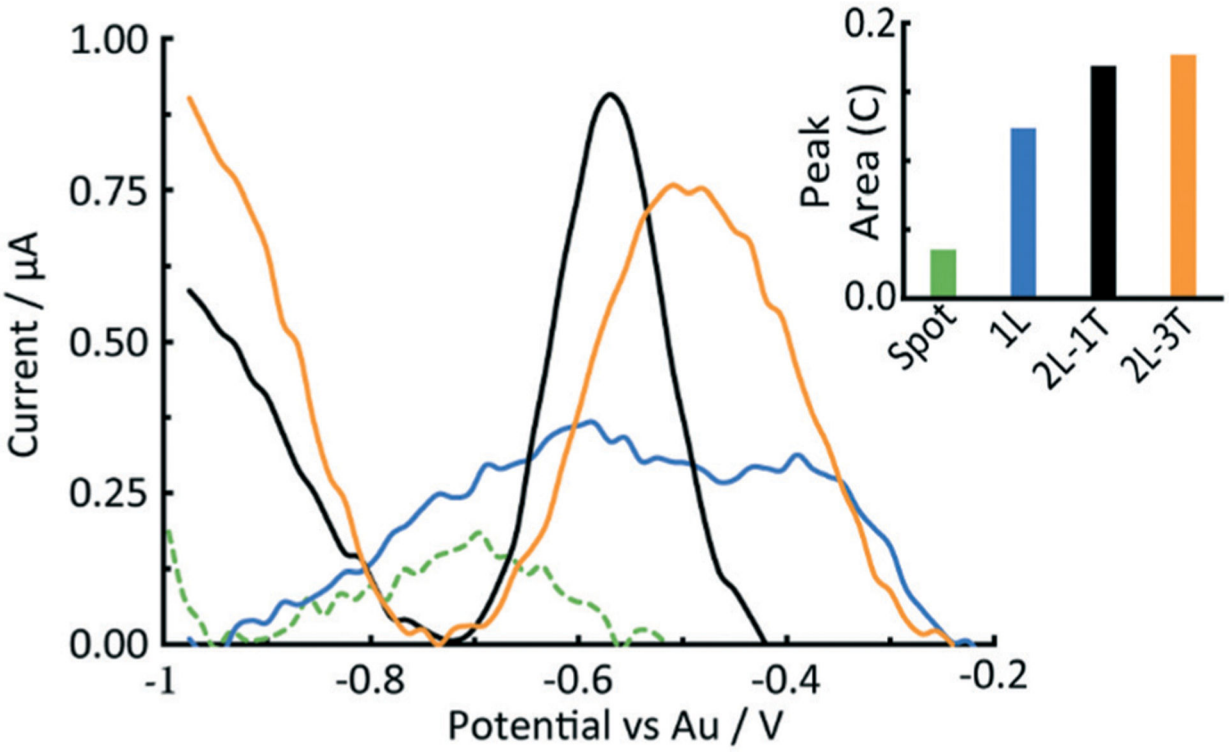

Fig. 8.

Square wave anodic stripping voltammetry of 400 ppm cadmium in a spot test (green, ‘spot’), a 1 layer of paper 3DPN (blue, ‘1L’), a 2 layers of paper 3DPN with 1 layer of tape (black, ‘2L-1T’), and a 2 layers of paper 3DPN with 3 layers of tape (orange, ‘2L-3T’) devices. All electrodes were Au microwires in a 3-electrode format spaced 1 mm apart in the channel between the paper layers or on top of the stationary spot test. Inset, corresponding peak areas from the stripping square wave voltammograms.

Table 1

Literature examples of fast flow μPADs, where v_x is the velocity, and V_f is the volumetric flow rate. Note channel cross sections are estimated based on the air gap around the paper/between paper layers and assuming negligible flow through the paper itself. This may overestimate v_x and underestimate V_f for devices where significant fluid is transported through the paper, such as the syringe pump driven flow[12,33]

Method	v_x/cm s^{-1}	V_f/mL min^{-1}	Ref.
2-layer μPAD with controlled channel height (passive)	1.56	1.65	This work
Syringe pump driven flow in blade cut paper channels	22	0.10	15, 16
Hollow channel between paper and wax, 4 mbar inlet pressure	1.2	0.21	18, 22
Hollow channel between paper and wax, 0.4 mbar inlet pressure	0.89	3.9×10^{-3}	54
Syringe pump driven flow in hollow channel between paper and PDMS	0.40	3.8×10^{-3}	53
1-layer μPAD (passive)	0.19	4.5×10^{-3}	17
2-layer μPAD with unfixed channel height (passive)	0.020	7.1×10^{-6}	9

Table 2

Effect of paper type on flow rate for vertical straight channel μPADs, where 3 layers of tape between the two paper layers ($n = 5$), v_X is the mean velocity, SD is the standard deviation, h is the paper thickness and r is the pore size[55]

Paper type	v_x/cm s^{-1}	SD	r/μm	h/μm
Whatman 1 chromatography	0.071	0.012	11	180
Whatman 1 quantitative	0.053	0.004	11	180
Whatman 4 qualitative	0.058	0.009	22.5	205